HHS Public Access

Author manuscript

J Cell Physiol. Author manuscript; available in PMC 2015 August 07.

Published in final edited form as:

J Cell Physiol. 2015 February ; 230(2): 337–346. doi:10.1002/jcp.24709.

Characterization of Cardiac Anoctamin1 Ca^{2+}-Activated Chloride Channels and Functional Role in Ischemia-Induced Arrhythmias

Zhen Ye[1], **Ming-Ming Wu**[1], **Chun-Yu Wang**[1], **Yan-Chao Li**[1], **Chang-Jiang Yu**[1], **Yuan-Feng Gong**[1], **Jun Zhang**[1], **Qiu-Shi Wang**[1], **Bin-Lin Song**[1], **Kuai Yu**[2], **H. Criss Hartzell**[2], **Dayue Darrel Duan**[3,*], **Dan Zhao**[1,**], and **Zhi-Ren Zhang**[1,**]

[1]Departments of Clinical Pharmacy and Cardiology, The 2nd Affiliated Hospital, Harbin Medical University, Key Laboratories of Education Ministry for Myocardial Ischemia Mechanism and Treatment, Harbin, P. R. China

[2]Department of Cell Biology, Emory University School of Medicine, Atlanta, Georgia

[3]Laboratory of Cardiovascular Phenomics, Department of Pharmacology, Center for Molecular Medicine, School of Medicine University of Nevada, Reno, Nevada

Abstract

Anoctamin1 (ANO1) encodes a Ca^{2+}-activated chloride (Cl^-) channel (CaCC) in variety tissues of many species. Whether ANO1 expresses and functions as a CaCC in cardiomyocytes remain unknown. The objective of this study is to characterize the molecular and functional expression of ANO1 in cardiac myocytes and the role of ANO1-encoded CaCCs in ischemia-induced arrhythmias in the heart. Quantitative real-time RT-PCR, immunofluorescence staining assays, and immunohistochemistry identified the molecular expression, location, and distribution of ANO1 in mouse ventricular myocytes (mVMs). Patch-clamp recordings combined with pharmacological analyses found that ANO1 was responsible for a Ca^{2+}-activated Cl^- current ($I_{Cl.Ca}$) in cardiomyocytes. Myocardial ischemia led to a significant increase in the current density of $I_{Cl.Ca}$, which was inhibited by a specific ANO1 inhibitor, $T16A_{inh}$-A01, and an antibody targeting at the pore area of ANO1. Moreover, cardiomyocytes isolated from mice with ischemia-induced arrhythmias had an accelerated early phase 1 repolarization of action potentials (APs) and a deeper “spike and dome” compared to control cardiomyocytes from non-ischemia mice. Application of the antibody targeting at ANO1 pore prevented the ischemia-induced early phase 1 repolarization acceleration and caused a much shallower “spike and dome”. We conclude that ANO1 encodes CaCC and plays a significant role in the phase 1 repolarization of APs in mVMs. The ischemia-induced increase in ANO1 expression may be responsible for the increased density of $I_{Cl.Ca}$ in the ischemic heart and may contribute, at least in part, to ischemia-induced arrhythmias.

[*]Correspondence to: Dayue Darrel Duan, Laboratory of Cardiovascular Phenomics, Department of Pharmacology, Center for Molecular Medicine, School of Medicine University of Nevada, Reno, NV 89557, dduan@medicine.nevada.edu. [**]Correspondence to: Dr. Zhi-Ren Zhang and Dr. Dan Zhao, Departments of Clinical Pharmacy and Cardiology, The 2nd Affiliated Hospital, Harbin Medical University, Key Laboratories of Education Ministry for Myocardial Ischemia Mechanism and Treatment, Harbin 150086, P. R. China. zhaod@rocketmail.com.

Zhen Ye and Ming-Ming Wu contributed equally to this work.

A calcium (Ca^{2+})-sensitive voltage-gated chloride (Cl^-) current ($I_{Cl.Ca}$) with distinct biophysical properties to classic Ca^{2+}-activated Cl^- channels (CaCCs) has been described in atrial and ventricular cardiomyocytes of several species (Duan et al., 2005; Duan, 2009), including swine (Li et al., 2003, 2004), canine (Tseng and Hoffman, 1989; Yue et al., 1997), rabbit (Zygmunt and Gibbons, 1991, 1992; Sipido et al., 1993; Wang et al., 1995), mouse (Xu et al., 2002), and human (Wang et al., 1995). It was reported that Cl^- channel blockers niflumic acid and 4,4′-diisothiocyanostilbene-2,2′-disulfonic acid (DIDS) (Li et al., 2003), or replacement of external Cl^- with methanesulfonate (Wang et al., 1995) resulted in an increase in APD. It was also suggested that $I_{Cl.Ca}$ may likely contribute to the rate- and rhythm-dependent repolarization of the cardiac action potential (AP) depending on intracellular Ca^{2+} activities (Zygmunt, 1994). In normal heart, however, $I_{Cl.Ca}$ may play an insignificant role in regulation of the diastolic membrane potential and action potential duration (APD) since the resting intracellular Ca^{2+} concentration ($[Ca^{2+}]_i$) is low under physiological conditions. But, when $[Ca^{2+}]_i$ is substantially increased above the physiological resting level, $I_{Cl.Ca}$ may carry a significant amount of transient outward current. It was proposed that under Ca^{2+} overload conditions $I_{Cl.Ca}$ may contribute to the arrhythmogenic transient inward current (IT) and cause delayed after depolarization (DAD). However, it remains unknown about the molecular identity and the exact physiological and pathophysiological role of CaCCs in the heart (Duan et al., 2005; Duan, 2009).

Recently, two members of the anoctamin (ANO) transmembrane protein family, ANO1 and ANO2, were determined to function as CaCCs in mouse over-expressed in *Axolotl* oocytes and HEK293 cells (Schroeder et al., 2008). Mouse ANO1 (mANO1) is broadly expressed in tissues known to contain native CaCCs. The human ANO1 mRNA is present in multiple human tissues including heart, lung, placenta, liver, skeletal muscle, and small intestine (Huang et al., 2006). The ANO1 (or TMEM16A)-encoded CaCC may participate in the control of cellular excitability, and regulation of smooth muscle contraction, slow wave activity in the gut, and fluid and salt transport by epithelia (Caputo et al., 2008; Schroeder et al., 2008; Yang et al., 2008; Duran and Hartzell, 2011). In this study, we investigated whether ANO1 underlies $I_{Cl.Ca}$ in mouse ventricular myocytes (mVMs) and whether it plays a functional role in ischemia-induced alteration of APD and arrhythmias in the heart.

Materials and Methods

Animals

All BALB/c mice (6–8 week, male, 20–25 g) were purchased from Experimental Animal Center of Harbin Medical University (HMU). This investigation conforms to the Guide for the Care and Use of Laboratory Animals (US NIH publication No. 85–23, revised 1996) and was in accordance with the institutional guidelines for animal care and use approved by the HMU Animal Supervision Committee.

Myocardial ischemia model

Mice were anesthetized with isoflurane (1–1.5% in medical oxygen) and intubated and mechanically ventilated. The chest was opened via an intercostals thoracotomy and ligation of the left anterior descending coronary arteries (LAD) was performed as previously

described (Xiang et al., 2011). The chest was closed and mouse was removed from the ventilator followed by recovery on a warm surface. Sham-operated animals received all procedures described above except actual ligation of the LAD. Electrocardiogram (ECG) recordings and Evan's blue staining (data not shown) were used to confirm establishment of myocardial ischemia and the ischemia-induced arrhythmias) (Bozeat et al., 2011).

Ventricular myocytes isolation and hypoxic exposure

Ventricular myocytes were freshly isolated from the left ventricle (LV) of the mice as previously described (Xu et al., 2002). Langendorff perfusion with Ca^{2+}-free Tyrode solution (mmol/L: 135 NaCl, 4.0 KCl, 0.33 NaH_2PO_4, 1.0 $MgCl_2 \cdot 6H_2O$, 10 HEPES, 10 glucose, and 10 BDM, pH 7.2 with NaOH) for 5 min, followed by 10 min perfusion with 0.3 mg/ml of collagenase B (Sigma, St. Louis, MO) and 0.6% bovine serum albumin (Promega, Mannheim, Germany). LV was separated, minced and incubated in a shaking bath for 5–10 min in collagenase-containing solutions. Cells were then harvested, washed twice, and stored in a high-K^+ storage solution (mmol/L: 30 KCl, 10 KH_2PO_4, 70 glutamic, 0.5 $MgCl_2$, 15 tourine, 10 HEPES, 0.5 EGTA, 10 glucose, pH7.4 with KOH) at 4 °C. Only rod-shaped ventricular myocytes showing clear cross striations were used for the following experiments. For hypoxic exposure, acutely isolated ventricular myocytes were placed in a hypoxic cell culture chamber (Thermo Scientific Series WJ 8000), and were kept at 37 °C for 30 min with a constant stream of water-saturated 92% N_2, 5% CO_2, and 3% O_2.

Patch-clamp recordings

The whole-cell patch-clamp configuration was used for AP and whole-cell current recordings as previously described (Huang et al., 2010) at room temperature (22–24 °C), using an Axopatch 200B amplifier (Axon Instruments, Foster City, CA) and data were filtered at 1 kHz and sampled at 5 kHz. Whole-cell current was elicited from a holding potential of −50 mV to voltage steps between −50 and +60 mV for 200 ms. Borosilicate glass electrodes had a resistance of 1–2 MΩ when filled with pipette solution containing (mmol/L) 110 Cesium Aspartate, 20 CsCl, 1 $MgCl_2$, 0.02 EGTA, 0.1 GTP, 5 ATP-Mg, 10 HEPES, and 5 Na_2-phosphocreatine (pH 7.4 with CsOH). Bath solution contained (mmol/L) 126 NMDG-Cl, 5.4 CsCl, 1 $MgCl_2$, 2 $CaCl_2$, 0.33 NaH_2PO_4, 10 dextrose, and 10 HEPES (pH 7.4 with CsOH). The cell capacitance was calculated by integrating the area under an uncompensated capacitive transient during voltage-clamp experiments. The peak current value of the whole-cell currents were normalized to cell capacitances (current density, pA/pF). For anion selectivity experiments, the extracellular 126 mM NMDG-Cl was replaced by equimolar NMDG-gluconate or NMDG-SCN and the data were corrected for junction potentials at the ground bridge (3 mmol/L KCl in 3% agar), which ranged from 2–4 mV as determined with a free-flowing KCl electrode. Reversal potentials (E_{rev}) for Cl^- and each test anions were used to calculate relative permeability (P_x/P_{Cl^-}) according to the Goldman-Hodgkin-Katz equation (Hille, 1986).

APs were recorded in mVMs using current clamp mode with a train of 40 super threshold square wave stimuli with 2-ms duration with stimulation frequencies of 5 Hz. For AP recordings, the extracellular solution contained (mmol/L) 126 NaCl, 2 $CaCl_2$, 5.4 KCl, 0.8 $MgCl_2$, 0.33 NaH_2PO_4, 10 dextrose, and 10 HEPES (pH 7.4 with NaOH) and the pipette

solution contained (mmol/L): 0.1 GTP, 110 potassium aspartate, 20 KCl, 1 $MgCl_2$, 5 ATP-Mg, 10 HEPES, 5 Na_2-phosphocreatine, and 0.05 EGTA (pH 7.4 with KOH) as previously used (Yue et al., 1997). The resting membrane potential of mVMs was adjusted to −60 ± 2 mV.

Quantitative real-time RT-PCR assays

Quantitative real-time RT-PCR (qRT-PCR) analyses were performed to examine the mRNA expression profiles of ANO1 and ANO2 in LV tissues. Briefly, Total mRNA was prepared from LV tissues by Trizol (Invitrogen, Carlsbad, CA) according to the manufacturer's instructions. The extracted total RNA was subjected to DNase treatment using the Turbo DNA-free kit (Ambion, Applies Biosystems, Foster City, CA). RNA (0.5 μg) was reverse transcribed using random primer and PrimeScript RT Master Mix (TAKARA, Shanghai, China) under 37 °C for 15 min. Quantitative real-time RT-PCR (qRT-PCR) analyses were performed in a Light Cycler (Roche Diagnostics, Germany), using the SYBR Premix Ex TaqTM (TAKARA, Shanghai, China). After activation of the Taq polymerase for 10 min at 95 °C, the amplification was followed by 20 sec at 95 °C, 20 sec at 55 °C, and 1 min at 72 °C for 50 cycles. The amplification was followed by a melting curve analysis to control of the PCR products. Analysis of the data was performed using Light Cycler software 3.5.3. The ratio for the amount of ANOs to GAPDH was calculated for each sample and analysis was performed in triplicates. The primers used for qRT-PCR are listed in Table 1.

Western blot analysis

Western blot, immunohistochemistry, and immunofluorescence staining were employed to examine the expression, distribution and localization of ANO1, using a specific anti-ANO1 antibody (Yu et al., 2010). Proteins (100 μg) extracted from isolated ventricular myocytes of LV were first separated by SDS-PAGE on 10% polyacrylamide gels and then transferred electrophoretically onto nitrocellulose membranes. Nonspecific binding sites were blocked with 5% nonfat milk powder in TBS-T (20 mM Tris-HCl pH 7.5, 137 mM NaCl, 0.1% Tween 20) for 2 h at 22–24 °C. The membranes were incubated overnight with the primary anti-ANO1 antibody against amino acid 878–960 (Yu et al., 2010) (1:1000 dilution) at 4 °C. After washing with TBS-T (3 × 5 min), blots were incubated with the HRP-conjugated goat anti-rabbit antibody (Invitrogen 62–6120, 1:5000 dilution) in TBS-T containing 1% nonfat milk powder for 60 min. After washing with TBS-T (3 × 5 min), bands were detected using enhanced chemiluminescence (Invitrogen, WP20005) and quantified by scanning densitometry (Bio-Rad Laboratories, Richmond, CA), the intensities of interesting band were normalized to the intensity of the β-actin band (Santa Cruz sc-47778).

Immunohistochemistry and immunofluorescence staining

Mouse heart was fixed in with 4% paraformaldehyde for 2 hrs followed by 18% sucrose for 16 hrs, then preserved in optimum cutting temperature compound (−80°C). Sections were cut with a Leica CM 3500 cryostat at a thickness of 4 μm. Isolated LV myocyte suspensions were placed on 12-mm glass coverslips pretreated with 10 μg/ml laminin for 30 min waiting for the cells adhesion. Heart tissue sections and LV myocytes were then fixed and permeablized with 4% buffered paraformaldehyde and 0.3% Triton X-100 for 20 min at 22 – 24°C. Blocking of nonspecific binding was accomplished by incubating in 1% BSA in PBS.

ANO1 labeling was performed by incubation with primary antibody against ANO1 (Yu et al., 2010) (1:1000 dilution) at 4 °C overnight and subsequent incubation with TRITC-conjugated secondary antibody (Zhongshan Golden Bridge Biotechnology ZF-0316, 1:2000 dilution) for 1 h. Identical acquisition settings were used on all images visualized by confocal microscope (Olympus Fluoview1000, Japan).

Data analyses

Data are reported as mean ± SEM. SigmaStat 3.5 software (Jandel Scientific, San Rafael, CA) and Student's t-tests for paired or unpaired data were used for statistical analysis. $P < 0.05$ was considered statistically significant.

Results

Expression, localization, and distribution of ANO1 in mouse ventricular tissues and myocytes

As shown in Figure 1A, only ANO1, but not ANO2, mRNA was expressed in mouse LV (Fig. 1A). Therefore, we focused on examining the localization and distribution of ANO1 in left ventricular tissues and myocytes. Immunofluorescence staining demonstrated that ANO1 was evenly distributed in the left ventricular epicardium and endocardium (Fig. 1B). Furthermore, immunocytochemistry clearly shows that ANO1 expresses in mVMs and is present in the vicinity of the plasma membrane of mVMs (Fig. 1C,a); ANO1 was also co-localized with α-actinin at the plasma membrane of mVM (Fig. 1C,b). The fluorescence intensity measured by line-scanning also suggested that ANO1 was more abundant at the plasma membrane of mVM (Fig. 1C,c).

The transient outward current is mediated by ANO1 in mVMs

All whole-cell currents were obtained using a voltage protocol as shown in the inset of Figure 2 in the presence of $BaCl_2$ (0.5 mmol/L), 4-AP (5 mmol/L), and TEA (10 mmol/L) in extracellular solutions to block potential K^+ currents including I_{K1}, $I_{to.1}$, and $I_{K.ur.}$ (Yue et al., 1997; Xu et al., 2002). A transient outward whole-cell current was detected in the mVMs under these conditions (Fig. 2A,a). The current was significantly blocked by a non-specific Cl^- channel blocker DIDS (150 μmol/L) in a voltage-dependent manner (Figs. 2A,b and c). Moreover, this current was significantly inhibited by extracellular application of a specific ANO1 inhibitor $T16A_{inh}$-A01 (Millipore, 613551) (Namkung et al., 2011; Davis et al., 2013) (Figs. 2B,b and c) and was also significantly inhibited by extracellular application of a specific pore-targeting anti-ANO1 antibody (1:100 dilution; Figs. 2C,b and c) (Thomas-Gatewood et al., 2011; Wu et al., 2014). In contrast, this current was not inhibited by either the boiled specific pore-targeting anti-ANO1 antibody (1:100 dilution) or the non-pore-targeting anti-ANO1 antibody (1:100 dilution; Figs. 2D,a–d) (Yu et al., 2010). These results strongly suggest that this transient outward whole-cell current in the mVMs is mediated by ANO1 (I_{ANO1}).

Cl^--dependence of the ANO1 current in mVMs

To further test whether the current was carried by Cl^-, the extracellular Cl^- was substituted by equimolar gluconate or SCN^-. The outward current density was reduced significantly by

replacing Cl^- with gluconate$^-$, and the reversal potential (E_{rev}) shifted toward positive potentials (Fig. 3A). Substitution of Cl^- with SCN^-, however, resulted in a significant increase in the magnitude of the outward current and the E_{rev} shifted toward negative potential (Fig. 3B). The relative permeability ratios for P_{gluc}/P_{Cl} and P_{SCN}/P_{Cl} were 0.11 ± 0.06 and 2.34 ± 0.12, respectively. All these properties of I_{ANO1} are consistent with those of CaCCs in many other cell types (Zygmunt and Gibbons, 1992; Valverde et al., 2010; Duran and Hartzell, 2011). These results strongly support the notion that I_{ANO1} in mVMs is carried by a Cl^- channel.

Ca^{2+}-dependent activation of the ANO1 Cl^- current in mVMs

The activation of I_{ANO1} Cl^- current was significantly decreased by extracellular application of nifedipine (5 μmol/L), an L-type calcium channel blocker (Fig. 4A). The current density was also dramatically decreased by applying extracellular caffeine (10 μmol/L) plus intracellular BAPTA (10 μmol/L in the pipette solution to deplete cytoplasmic Ca^{2+}) (Fig. 4B). These results suggest that activation of the ANO1 Cl^- current in mVMs is dependent on Ca^{2+} entry-induced increase in intracellular Ca^{2+} concentrations.

Effects of myocardial ischemia on ANO1 Cl^- current in mVMs

We hypothesized that the Ca^{2+}-activated ANO1 Cl^- current (ANO1 $I_{Cl.Ca}$) would be significantly amplified under conditions with $[Ca^{2+}]_i$ overload in mVMs during ischemia (Valverde et al., 2010). As shown in Figure 5, $I_{Cl.Ca}$ was significantly increased in the mVMs isolated from myocardial ischemia area (Figs. 5A,b and 5B,b) compared to that in sham mice (Figs. 5A,a and 5B,a). These ischemia-enhanced $I_{Cl.Ca}$ was dramatically inhibited by the specific pore-targeting anti-ANO1 antibody and $T16A_{inh}$-A01, respectively (Figs. 5A,c and 5B,c). Similarly, mVMs exposed to hypoxia (3% O_2 for 30 min) also caused a significant increase in $I_{Cl.Ca}$, which was also inhibited by either the specific pore-targeting anti-ANO1 antibody (Fig. 6A,c) or $T16A_{inh}$-A01 (Fig. 6B,c). These results strongly support that myocardial ischemia or hypoxia causes an increase in the ANO1 $I_{Cl.Ca}$ in mVMs.

Expression profile of ANO1 in ischemic mVMs

As shown in Figure 7A, myocardial ischemia caused a significant increase in ANO1 mRNA expression in LV tissues. Western blot analysis also showed that the abundance of ANO1 in mVMs isolated from the ischemic region was significantly greater than in those from control or sham group (Fig. 7B). These results suggest that the ischemia/hypoxia-induced increase in the functional ANO1 $I_{Cl.Ca}$ may be a result of an increased expression of ANO1.

Functional role of ANO1 $I_{Cl.Ca}$ in the regulation of action potential duration (APD)

Theoretically, activation of $I_{Cl.Ca}$ should play an important role in the phase 1 repolarization of APD (Duan et al., 2005; Duan, 2009), as suggested for $I_{Cl.Ca}$ in rabbit atrial myocytes (Wang et al., 1995) and pig ventricular myocytes (Li et al., 2003). As shown in Figure 8 the phase 1 repolarization of APs recorded from mVMs, isolated from myocardial ischemia area of the mice underwent the arrhythmias (Fig. 8A), is much faster than that recorded from sham group (Figs. 8B,a and b; Table 2). In contrast, the phase 1 repolarization of APs was significantly retarded by the specific pore-targeting ANO1 antibody (Figs. 8C,a and b; Table

2) or the specific ANO1 inhibitor $T16A_{inh}$-A01 (data not shown). The time constants (τ), obtained by fitting the repolarization of APs from the peak of "spike" to the beginning of "dome" using a single exponential function, also revealed that ischemia accelerated the early phase 1 of repolarization and that the specific pore-targeting ANO1 antibody retarded early phase 1 of repolarization (Table 3).

Discussion

The major findings of the present study include: (1) ANO1 was expressed and widely distributed in mouse heart; (2) ANO1 was localized at the plasma membrane of the mVMs; (3) ANO1 functions as $I_{Cl.Ca}$ in cardiac myocytes; (4) the ANO1 $I_{Cl.Ca}$ may play a crucial role in the phase 1 repolarization and thus the regulation of cardiac APD; (5) myocardial ischemia caused a significant upregulation of the expression of ANO1 at both molecular and functional levels, which may contribute significantly to ischemia-induced arrhythmias in the mouse heart.

Molecular and functional expression of ANO1 in mouse heart and mVMs

Previous studies have suggested that both ANO1 and ANO2 of the ANO family form endogenous CaCCs in several cell types (Schroeder et al., 2008; Manoury et al., 2010; Romanenko et al., 2010; Dutta et al., 2011; Thomas-Gatewood et al., 2011). To date the molecular expression of ANO1 and ANO2 and their relationships to CaCCs (or $I_{Cl.Ca}$) in the heart remains unknown. Our data demonstrated that ANO1, but not ANO2, was expressed in the plasma membrane of the mVMs (Fig. 1). Furthermore, we found the specific ANO1 inhibitor $T16A_{inh}$-A01 significantly inhibited the whole-cell currents in the mVMs (Fig. 2B). In addition, a specific anti-ANO1 antibody targeting at the predicted pore-forming region (Yang et al., 2008) was also able to effectively block the whole-cell current when delivered to the cell (Fig. 2C). These results are consistent with the inhibitory effects of the same anti-ANO1 antibody on $I_{Cl.Ca}$ in rat cerebral artery smooth muscle cells (Thomas-Gatewood et al., 2011). It has been known that mouse and rat ANO1s are nearly identical in amino acid sequence and are predicted to share similar genomic and phenotypic features (Hartzell et al., 2009). Moreover, the $T16A_{inh}$-A01 and specific pore-targeting anti-ANO1 antibody-sensitive whole-cell current (I_{ANO1}) can also be effectively blocked by Cl^- channel blocker DIDS (Fig. 2A). Changes in the transmembrane Cl^- gradients shifted the E_{rev} of the I_{ANO1}, as predicted for a typical Cl^- channel. The anion selectivity data showed that the relative permeability for SCN^- (~2.34) > Cl^- > gluconate$^-$ (~0.11). The activation of the ANO1 Cl^- current is strongly dependent on the Ca^{2+}-entry induced Ca^{2+} release of intracellular Ca^{2+} (Fig. 4). These features are compatible to that observed in other native classical CaCCs (Zygmunt and Gibbons, 1992; Valverde et al., 2010; Duran and Hartzell, 2011). Therefore, these data together provide compelling evidence that, similar to its function in many other tissues, ANO1 expressed in the mouse heart also functions as a CaCC.

Properties of $I_{Cl.Ca}$ in the heart

Cardiac $I_{Cl.Ca}$ was first characterized by Zygmunt et al. in rabbit ventricular myocytes as a Ca^{2+}-dependent component of the transient outward current (I_{to}) (Zygmunt and Gibbons,

1991). In order to separate it from the 4-AP-sensitive transient outward K^+ current (I_{to1}) this $I_{Cl.Ca}$ was termed I_{to2}. Later, I_{to2} was also described in rabbit atrial (Zygmunt and Gibbons, 1992) and Purkinje cells (Sipido et al., 1993), canine ventricular cells (Tseng and Hoffman, 1989; Zygmunt, 1994; Collier et al., 1996), cultured embryonic chick cardiac cells (Liu and Lieberman, 1994) and human atrial myocytes (Escande et al., 1987; Sorota, 1999; Hume et al., 2000). One of the unique features of I_{to2} is the kinetic behavior and the bell-shaped I–V relationship because activation of I_{to2} is significantly determined by the time course of the $[Ca^{2+}]_i$ transient (Zygmunt and Gibbons, 1991). The time-dependent activation kinetics was abolished when $[Ca^{2+}]_i$ was "clamped" at a constant level and the I–V relationship became linear when the Cl^- gradient is symmetrical (Hume et al., 2000). More recently, Xu et al. characterized an I_{to2} in mouse heart and found that the I–V relationship of mouse cardiac I_{to2} was not bell-shaped (Xu et al., 2002). Therefore, the biophysical features of $I_{Cl.Ca}$ may be species-dependent or affected by different experimental conditions.

The whole-cell ANO1 $I_{Cl.Ca}$ recorded from mVMs in this study shares many biophysical and pharmacological features, including the blockade by DIDS, the dependence of activation upon Ca^{2+} influx via voltage-gated Ca^{2+} channels and release from intracellular Ca^{2+} stores, the I–V relationship, and the lack of voltage-dependent relaxation, with those of $I_{Cl.Ca}$ in the native mouse heart previously described by Xu et al (Xu et al., 2002).

Molecular property and functional role of $I_{Cl.Ca}$ in the heart

Normally, $I_{Cl.Ca}$ will have insignificant effects on the diastolic membrane potential, as resting $[Ca_{2+}]^i$ is low. When $[Ca_{2+}]^i$ is substantially increased above the physiological resting level, however, $I_{Cl.Ca}$ carries a significant amount of transient outward current. $I_{Cl.Ca}$ will activate early during the action potential in response to an increase in $[Ca^{2+}]_i$ associated with Ca^{2+}-induced Ca^{2+} release (CICR). The time course of decline of the $[Ca^{2+}]_i$ transient will determine the extent to which $I_{Cl.Ca}$ contributes to early repolarization during phase 1. In Ca^{2+}-overloaded cardiac preparations, $I_{Cl.Ca}$ can contribute to the arrhythmogenic transient inward current (I_{TI}) (Zygmunt, 1994). I_{TI} produces delayed after depolarization (DAD) and induces triggered activity, which is an important mechanism for abnormal impulse formation (January and Fozzard, 1988). In sheep Purkinje and ventricular myocytes, activation of $I_{Cl.Ca}$ was found to induce DAD and plateau transient repolarization (Verkerk et al., 2000). Therefore, blockade of $I_{Cl.Ca}$ may be potentially antiarrhythmogenic by reducing DAD amplitude and triggered activity based on DAD. Due to the lack of knowledge on the molecular properties of $I_{Cl.Ca}$ and specific pharmacological tools the role of $I_{Cl.Ca}$ in phase 1 repolarization and the generation of EAD and DAD of either normal or diseased heart and the clinical relevance of $I_{Cl.Ca}$ blockers remain to be determined (Verkerk et al., 2000; Duan, 2013).

In this study we found that the phase 1 repolarization was more rapid (Tables 2 and 3) and the "spike and dome" was deeper in mVMs isolated from ischemic area of hearts that underwent arrhythmias compared to control. The density of $I_{Cl.Ca}$ was substantially amplified in the mVMs from either ischemic region of heart or in the mVMs exposed to hypoxia in vitro. Application of the pore-targeting ANO1 antibody leads to a significantly retarded the phase 1 repolarization of APs (Tables 2 and 3) and results in a shallower "spike

and dome" of phase 1 repolarization. These results are consistent with those found in swine ventricular myocytes, where the phase 1 and "spike and dome" were abolished by DIDS (Li et al., 2003). Xu et al. observed that niflumic acid (NFA) significantly prolonged repolarization of APD in mVMs (Xu et al., 2002), this could be due to NFA is a non-specific Cl^- channel blocker. Although APD_{90} was significantly prolonged in mVMs isolated from ischemic area, it was unlikely due to activation of ANO1 because the pore-specific anti-ANO1 did not alter APD_{90} (Table 2).

The reasons for an increase in $I_{Cl.Ca}$ density under ischemic condition could be attributable to significantly increased ANO1 expression, the $[Ca^{2+}]_i$ overload due to excessive Ca^{2+} accumulation in sarcoplasmic reticulum and paralleling an increase in $[Ca^{2+}]_i$ (Valverde et al., 2010) and increased oxidative stress in ischemia heart tissue, because the enhanced level of H_2O_2 can reversibly or irreversibly activate CaCCs (Jeulin et al., 2005). The mechanism by which ischemia induces an enhanced ANO1 expression in ischemic heart is unknown. An inflammatory factor, IL-4, has shown to increase ANO1 protein expression, membrane localization, and transepithelial secretion of Cl^- in polarized epithelial cells (Dutta et al., 2011).

In conclusion, our results provide the very first experimental evidence suggests that ANO1 confers $I_{Cl.Ca}$ in mVMs and plays a role in early phase of repolarization of AP. Abnormal activation of ANO1 may contribute to ischemia-induced arrhythmias via affecting AP.

Clinical relevance

The novel findings of ANO1 in the heart and the functional role of ANO1 $I_{Cl.Ca}$ in the normal and ischemic heart provide new mechanistic insights into the ischemia-induced arrhythmias and also new therapeutic targets for the treatment of ischemia-induced arrhythmias.

Acknowledgments

This study was supported by Key Project of Chinese National Program for Fundamental Research and Development (973 Program 2012CB517803, 2014CB542401 to Z. Z.), NSFC (30871007, 81070217 to Z. Z.), Doctoral Tutor Foundation of Ministry of Education (20122307110008 to Z. Z.), the Natural Science Foundation of Heilongjiang Province (ZD200807-01, ZD200807-02 to Z. Z. and QC2010097 to D. Z.), Overseas Talent Foundation of Department of Education, Heilongjiang Province (1154HZ11 to Z. Z.), and Science Research Foundation of Graduate School of HMU (YJSCX2011-336 to Z. Y.). This study was also supported by AHA Western States Affiliate Grant-in-Aid (11GRNT7610161 to D. D.) and the NIH Grant (HL106256 to D. D.).

Literature Cited

Bozeat ND, Xiang SY, Ye LL, Yao TY, Duan ML, Burkin DJ, Lamb FS, Duan DD. Activation of volume regulated chloride channels protects myocardium from ischemia/reperfusion damage in second-window ischemic preconditioning. Cell Physiol Biochem: Int J Exp Cell Physiol Biochem Pharmacol. 2011; 28:1265–1278.

Caputo A, Caci E, Ferrera L, Pedemonte N, Barsanti C, Sondo E, Pfeffer U, Ravazzolo R, Zegarra-Moran O, Galietta LJ. TMEM 16A, a membrane protein associated with calcium-dependent chloride channel activity. Science. 2008; 322:590–594. [PubMed: 18772398]

Collier ML, Levesque PC, Kenyon JL, Hume JR. Unitary Cl^- channels activated by cytoplasmic Ca^{2+} in canine ventricular myocytes. Circ Res. 1996; 78:936–944. [PubMed: 8620614]

Davis AJ, Shi J, Pritchard HA, Chadha PS, Leblanc N, Vasilikostas G, Yao Z, Verkman AS, Albert AP, Greenwood IA. Potent vasorelaxant activity of the TMEM 16A inhibitor T16A(inh)-A01. Br J Pharmacol. 2013; 168:773–784. [PubMed: 22946562]

Duan D. Phenomics of cardiac chloride channels: The systematic study of chloride channel function in the heart. J Physiol. 2009; 587:2163–2177. [PubMed: 19171656]

Duan DD. Phenomics of cardiac chloride channels. Compr Physiol. 2013; 3:667–692. [PubMed: 23720326]

Duan DY, Liu LL, Bozeat N, Huang ZM, Xiang SY, Wang GL, Ye L, Hume JR. Functional role of anion channels in cardiac diseases. Acta Pharmacol Sin. 2005; 26:265–278. [PubMed: 15715921]

Duran C, Hartzell HC. Physiological roles and diseases of Tmem 16/Anoctamin proteins: Are they all chloride channels? Acta Pharmacol Sin. 2011; 32:685–692. [PubMed: 21642943]

Dutta AK, Khimji AK, Kresge C, Bugde A, Dougherty M, Esser V, Ueno Y, Glaser SS, Alpini G, Rockey DC, Feranchak AP. Identification and functional characterization of TMEM 16A, a Ca^{2+}-activated Cl^- channel activated by extracellular nucleotides, in biliary epithelium. J Biol Chem. 2011; 286:766–776. [PubMed: 21041307]

Escande D, Coulombe A, Faivre JF, Deroubaix E, Coraboeuf E. Two types of transient outward currents in adult human atrial cells. Am J Physiol. 1987; 252:H142–H148. [PubMed: 3028160]

Hartzell HC, Yu K, Xiao Q, Chien LT, Qu Z. Anoctamin/TMEM 16 family members are Ca^{2+}-activated Cl^- channels. J Physiol. 2009; 587:2127–2139. [PubMed: 19015192]

Hille B. Ionic channels: Molecular pores of excitable membranes. Harvey Lectures. 1986; 82:47–69. [PubMed: 2452140]

Huang X, Godfrey TE, Gooding WE, McCarty KS Jr, Gollin SM. Comprehensive genome and transcriptome analysis of the 11q13 amplicon in human oral cancer and synteny to the 7F5 amplicon in murine oral carcinoma. Genes Chromosomes Cancer. 2006; 45:1058–1069. [PubMed: 16906560]

Huang W, Zhang D, Millard RW, Wang T, Zhao T, Fan GC, Ashraf A, Xu M, Ashraf M, Wang Y. Gene manipulated peritoneal cell patch repairs infarcted myocardium. J Mol Cell Cardiol. 2010; 48:702–712. [PubMed: 19913551]

Hume JR, Duan D, Collier ML, Yamazaki J, Horowitz B. Anion transport in heart. Physiol Rev. 2000; 80:31–81. [PubMed: 10617765]

January CT, Fozzard HA. Delayed after depolarizations in heart muscle: Mechanisms and relevance. Pharmacol Rev. 1988; 40:219–227. [PubMed: 3065793]

Jeulin C, Guadagnini R, Marano F. Oxidant stress stimulates Ca^{2+}-activated chloride channels in the apical activated membrane of cultured nonciliated human nasal epithelial cells. Am J Physiol Lung Cell Mol Physiol. 2005; 289:L636–L646. [PubMed: 16148052]

Li GR, Du XL, Siow YLOK, Tse HF, Lau CP. Calcium-activated transient outward chloride current and phase 1 repolarization of swine ventricular action potential. Cardiovascular Res. 2003; 58:89–98.

Li GR, Sun H, To J, Tse HF, Lau CP. Demonstration of calcium-activated transient outward chloride current and delayed rectifier potassium currents in Swine atrial myocytes. J Mol Cell Cardiol. 2004; 36:495–504. [PubMed: 15081309]

Liu S, Lieberman M. Electrodiffusive movements of chloride ion in sodium-free solution: A possible calcium activated chloride conductance in cultured heart cells. Cardiovascular Res. 1994; 28:1629–1634.

Manoury B, Tamuleviciute A, Tammaro P. TMEM 16A/anoctamin 1 protein mediates calcium-activated chloride currents in pulmonary arterial smooth muscle cells. J Physiol. 2010; 588:2305–2314. [PubMed: 20421283]

Namkung W, Phuan PW, Verkman AS. TMEM 16A inhibitors reveal TMEM 16A as a minor component of calcium-activated chloride channel conductance in airway and intestinal epithelial cells. J Biol Chem. 2011; 286:2365–2374. [PubMed: 21084298]

Romanenko VG, Catalan MA, Brown DA, Putzier I, Hartzell HC, Marmorstein AD, Gonzalez-Begne M, Rock JR, Harfe BD, Melvin JE. Tmem 16A encodes the Ca^{2+}-activated Cl^- channel in mouse submandibular salivary gland acinar cells. J Biol Chem. 2010; 285:12990–13001. [PubMed: 20177062]

Schroeder BC, Cheng T, Jan YN, Jan LY. Expression cloning of TMEM 16A as a calcium-activated chloride channel subunit. Cell. 2008; 134:1019–1029. [PubMed: 18805094]

Sipido KR, Callewaert G, Carmeliet E. [Ca2+]i transients and [Ca2+]i-dependent chloride current in single Purkinje cells from rabbit heart. J Physiol. 1993; 468:641–667. [PubMed: 8254529]

Sorota S. Insights into the structure, distribution and function of the cardiac chloride channels. Cardiovascular Res. 1999; 42:361–376.

Thomas-Gatewood C, Neeb ZP, Bulley S, Adebiyi A, Bannister JP, Leo MD, Jaggar JH. TMEM 16A channels generate Ca(2)(+)-activated Cl(−) currents in cerebral artery smooth muscle cells. Am J Physiol Heart Circ Physiol. 2011; 301:H1819–H1827. [PubMed: 21856902]

Tseng GN, Hoffman BF. Two components of transient outward current in canine ventricular myocytes. Circ Res. 1989; 64:633–647. [PubMed: 2539269]

Valverde CA, Kornyeyev D, Ferreiro M, Petrosky AD, Mattiazzi A, Escobar AL. Transient Ca^{2+} depletion of the sarcoplasmic reticulum at the onset of reperfusion. Cardiovasc Res. 2010; 85:671–680. [PubMed: 19920131]

Verkerk AO, Veldkamp MW, Bouman LN, van Ginneken AC. Calcium-activated Cl(−) current contributes to delayed after depolarizations in single Purkinje and ventricular myocytes. Circulation. 2000; 101:2639–2644. [PubMed: 10840017]

Wang Z, Fermini B, Feng J, Nattel S. Role of chloride currents in repolarizing rabbit atrial myocytes. Am J Physiol. 1995; 268:H1992–H2002. [PubMed: 7771549]

Wu MM, Lou J, Song BL, Gong YF, Li YC, Yu CJ, Wang QS, Ma TX, Ma K, Hartzell HC, Duan DD, Zhao D, Zhang ZR. Hypoxia augments anoctamin 1-encoded calcium-activated chloride current in cardiac vascular endothelial cells of neonatal mouse. Br J Pharmacol. 2014

Xiang SY, Ye LL, Duan LL, Liu LH, Ge ZD, Auchampach JA, Gross GJ, Duan DD. Characterization of a critical role for CFTR chloride channels in cardioprotection against ischemia/reperfusion injury. Acta Pharmacol Sin. 2011; 32:824–833. [PubMed: 21642951]

Xu Y, Dong PH, Zhang Z, Ahmmed GU, Chiamvimonvat N. Presence of a calcium-activated chloride current in mouse ventricular myocytes. Am J Physiol Heart Circ Physiol. 2002; 283:H302–H314. [PubMed: 12063303]

Yang YD, Cho H, Koo JY, Tak MH, Cho Y, Shim WS, Park SP, Lee J, Lee B, Kim BM, Raouf R, Shin YK, Oh U. TMEM 16A confers receptor-activated calcium-dependent chloride conductance. Nature. 2008; 455:1210–1215. [PubMed: 18724360]

Yu K, Lujan R, Marmorstein A, Gabriel S, Hartzell HC. Bestrophin-2 mediates bicarbonate transport by goblet cells in mouse colon. J Clin Invest. 2010; 120:1722–1735. [PubMed: 20407206]

Yue L, Feng J, Gaspo R, Li GR, Wang Z, Nattel S. Ionic remodeling underlying action potential changes in a canine model of atrial fibrillation. Circ Res. 1997; 81:512–525. [PubMed: 9314832]

Zygmunt AC. Intracellular calcium activates a chloride current in canine ventricular myocytes. Am J Physiol. 1994; 267:H1984–H1995. [PubMed: 7977830]

Zygmunt AC, Gibbons WR. Calcium-activated chloride current in rabbit ventricular myocytes. Circ Res. 1991; 68:424–437. [PubMed: 1991347]

Zygmunt AC, Gibbons WR. Properties of the calcium-activated chloride current in heart. J Gen Physiol. 1992; 99:391–414. [PubMed: 1375275]

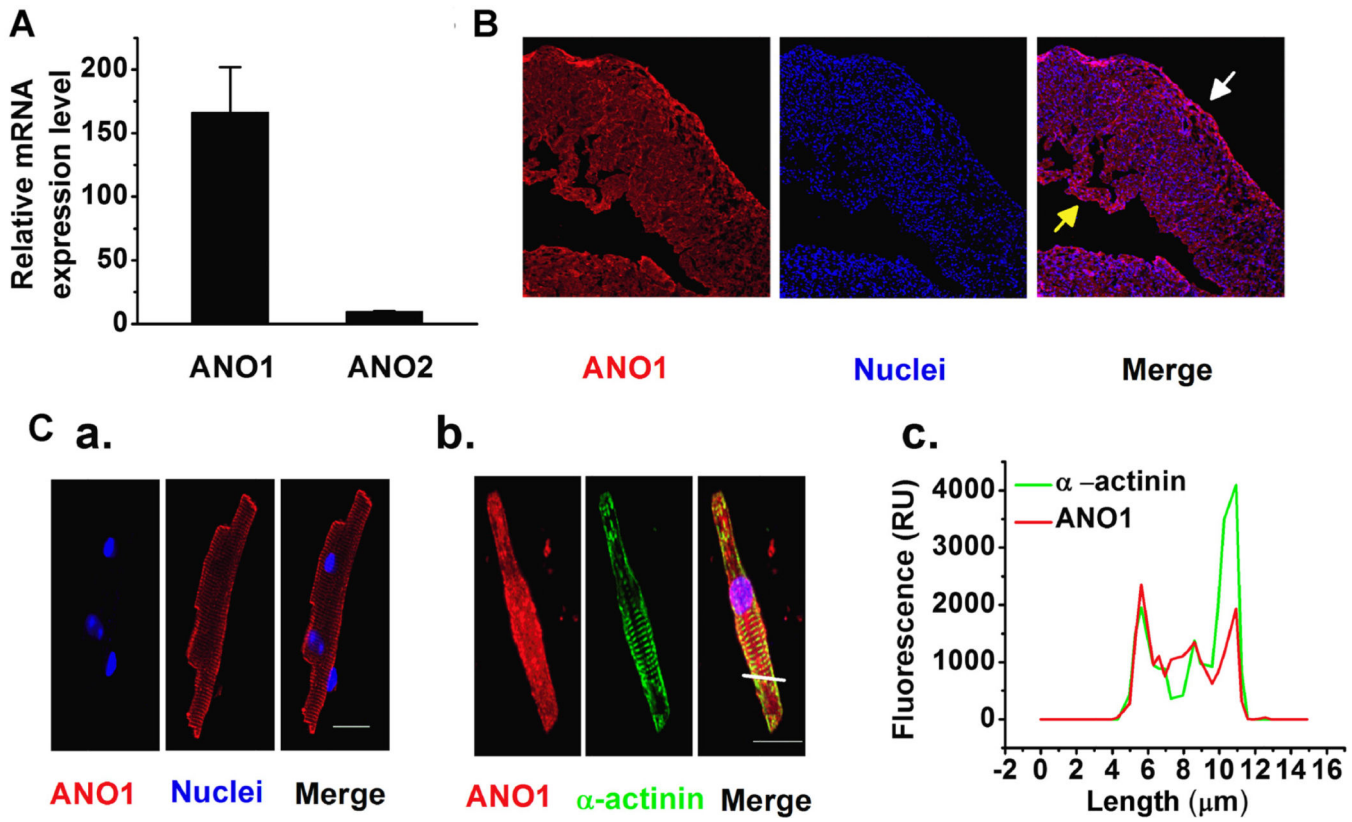

Fig. 1.

(A) qRT-PCR revealed that ANO1, but not ANO2 expressed in LV tissues (n = 3); (B) Representative immunohistochemistry images demonstrate that ANO1 distributes from epi- (the white arrow head), mid-myocardial and endocardial (the yellow arrow head) layers of the mouse LV. (C) Representative immunofluorescence staining images suggest that ANO1 is localized on the plasma membrane of the ventricular myocytes. Ventricular myocytes labeled with antibody against ANO1 (C,a; red), or co-labeled with antibodies raised against ANO1 (red) and against α-actinin (green) (C,b). Scale bars by white solid lines represent 20 μm. (C,c) The constructed histograms of fluorescence intensity across the cell (where indicated by the yellow solid line in C,b) for ANO1 (the red solid line) and α-actinin (the green solid line) suggest that ANO1 is mainly localized at the plasma membrane of mVMs (C,c).

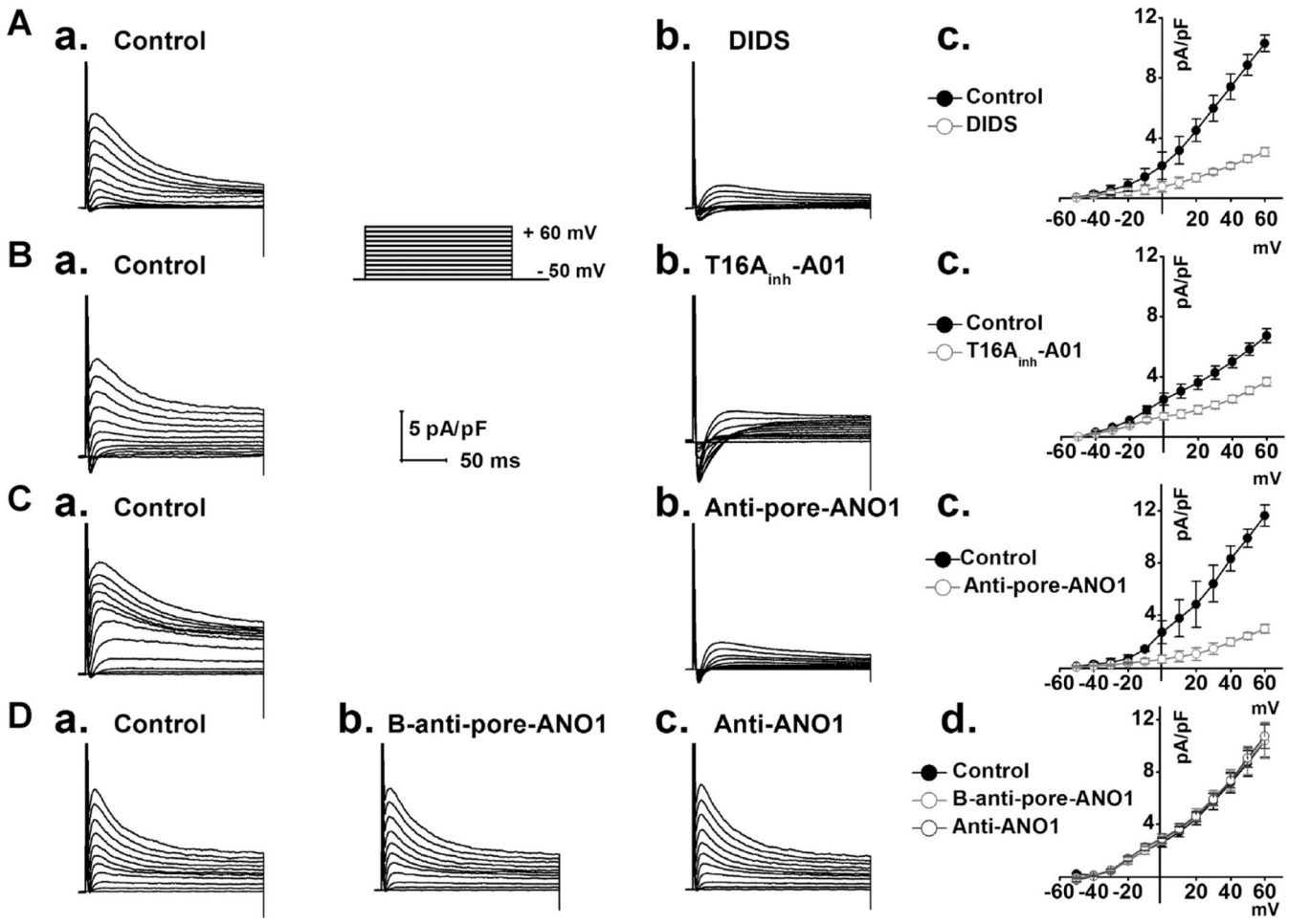

Fig. 2.

A. Representative whole-cell currents were recorded from control (A,a) and in the presence of 150 μmol L^{-1} DIDS (A,b); average I–V relationships (A,c) were constructed as a function of voltages from records as shown in A,a and A,b (n = 6). B. Representative whole-cell currents were recorded under control condition (B,a) and in the presence of 30 μmol L^{-1} specific ANO1 blocker T16A_{inh}-A01 (B,b); I–V relationships (B,c) were constructed against voltages from records as shown in B,a and B,b. (n = 5). C. Representative whole-cell currents were recorded under control condition (C,a) and in the presence of the specific pore-targeting anti-ANO1 antibody in the same ventricular myocyte (C,b); I–V relationships (C,c) were constructed as a function of voltages from records as shown in C,a and C,b (n = 5). D. Representative whole-cell currents were respectively recorded under control condition (D,a), in the presence of the boiled specific pore-targeting anti-ANO1 antibody (D,b) and in the presence of a non-pore-targeting anti-ANO1 antibody (D,c) ; I–V relationships (D,d) were constructed as a function of voltages from records as shown in D,a–c (n = 5). Anti-pore-ANO1, B-anti-pore-ANO1 and Anti-ANO1 respectively represent specific pore-targeting anti-ANO1 antibody, boiled specific pore-targeting anti-ANO1 antibody and non-pore-targeting anti-ANO1 antibody.

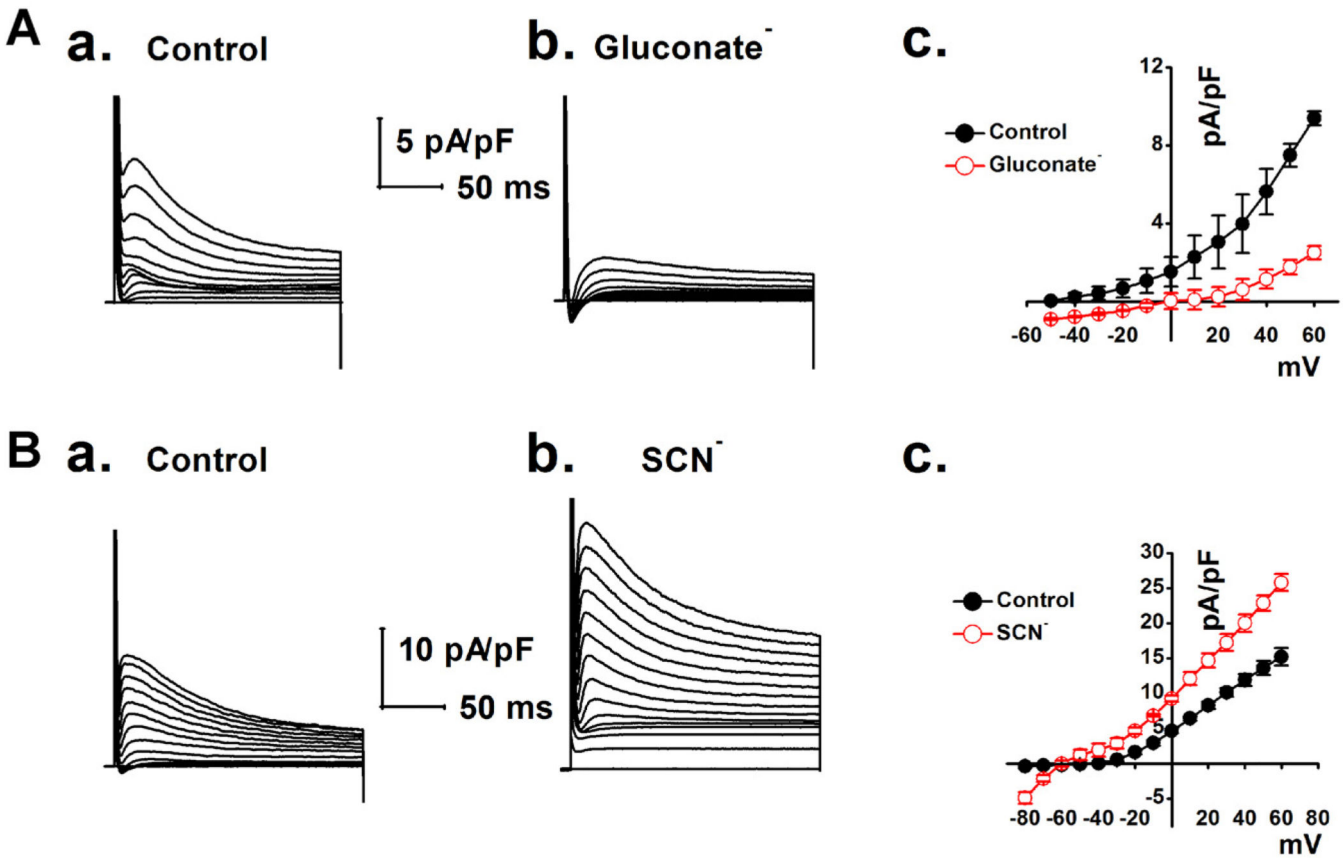

Fig. 3.

A. Representative whole-cell currents were recorded from control (A,a) and extracellular Cl^- substituted by equimolar $gluconate^-$ (A, b). I–V relationships demonstrated that replacement of Cl^- with $gluconate^-$ led to a significantly decreased density of the outward currents and the E_{rev} shifted toward more positive potentials (A,c) (n = 5). B. Representative whole-cell currents were recorded from control (B,a) and extracellular Cl^- replaced with equimolar SCN^- (B,b). I–V relationships showed that replacement of Cl^- with SCN^- resulted in a significantly increased density of the outward currents and the E_{rev} shifted toward more negative potentials (B,c) (n = 5).

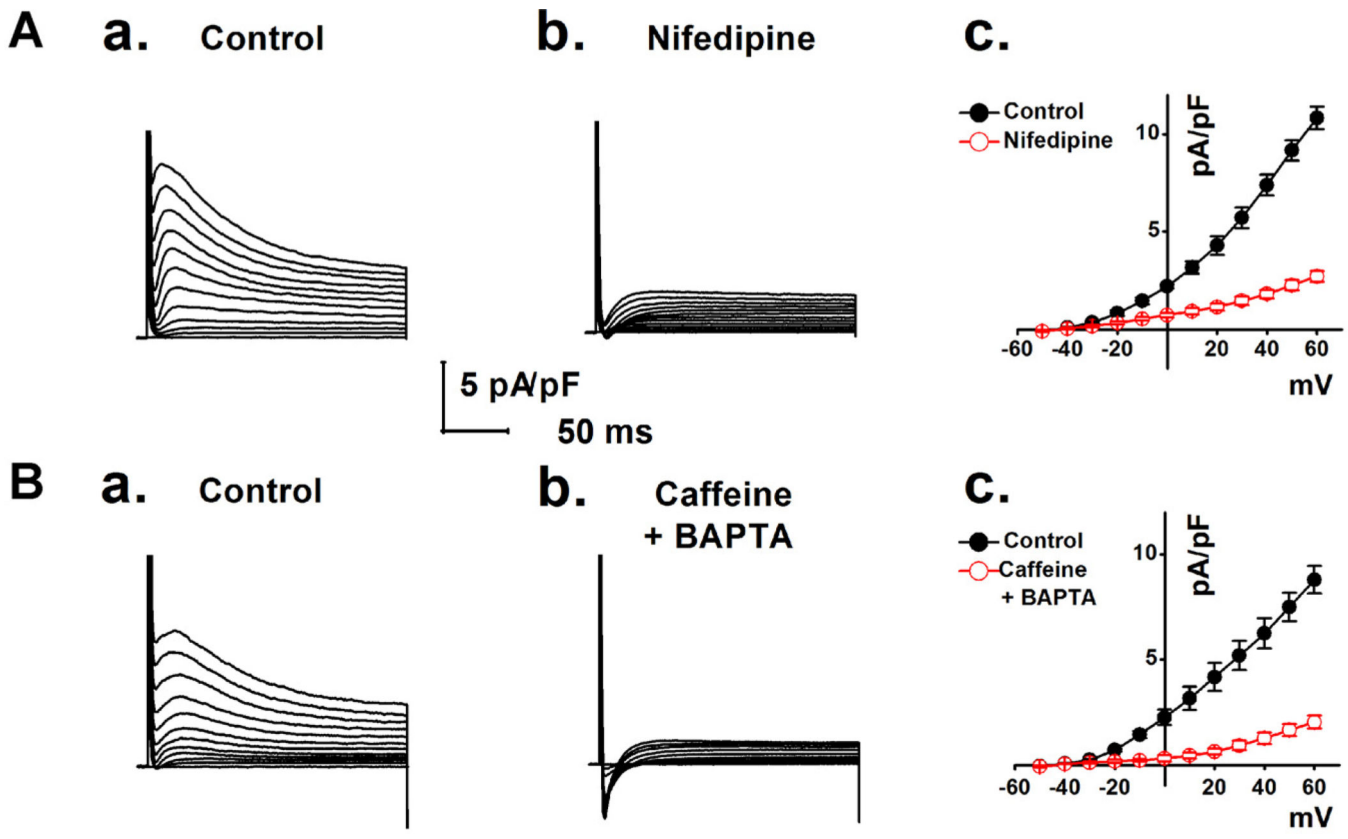

Fig. 4.

A. The representative macroscopic currents were recorded in the absence (A,a) or in the presence of 5 μmol L^{-1} nifedipine (A,b). I–V relationships from the records as shown in A,a and A,b are shown in panel A,c (n = 7). B. The representative whole-cell currents were recorded in the absence of (B,a) or in the presence of 10 μmol L^{-1} extracellular caffeine plus 10 mmol L^{-1} pipette BAPTA (B,b). Panel B,c shows the average I–V curves from the recordings (n = 6) as shown in B,a and B,b.

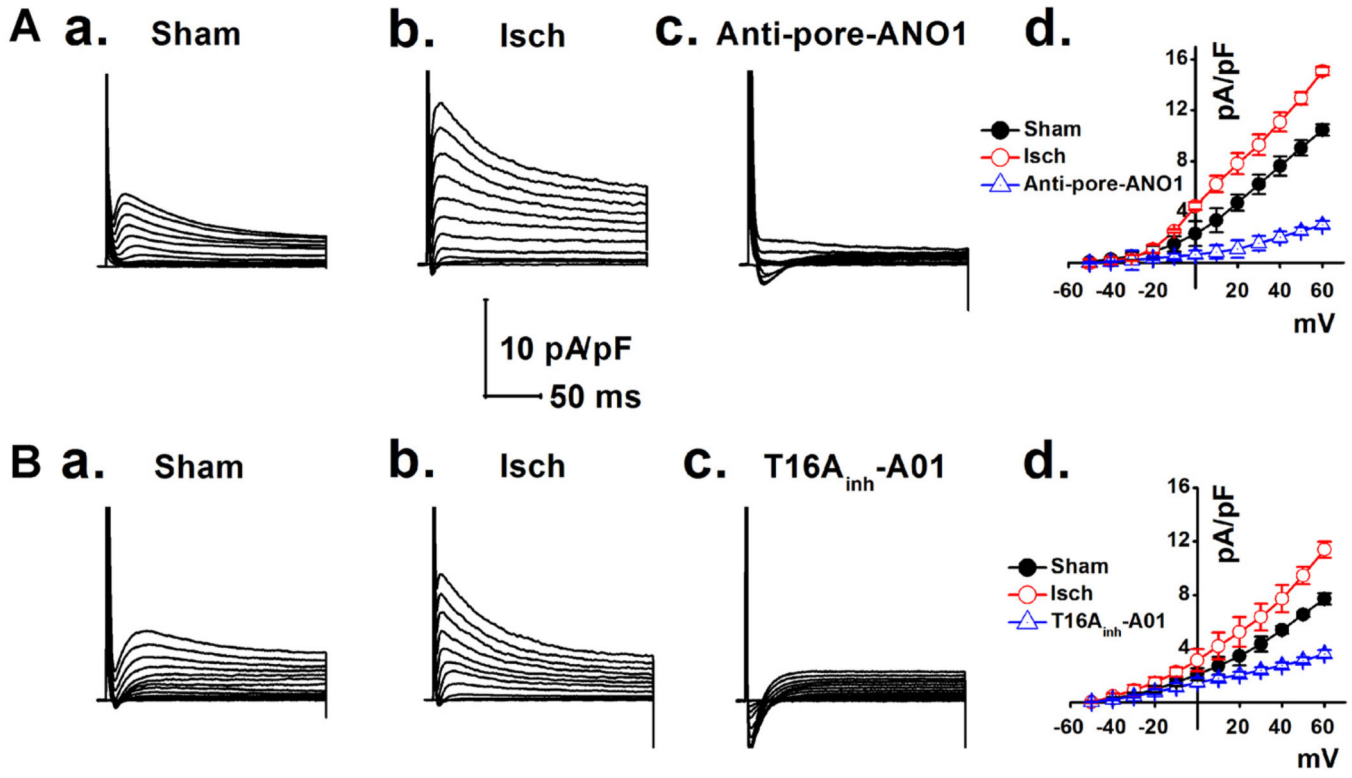

Fig. 5.

Ischemia-induced increase in $I_{Cl.Ca}$ in mVMs was respectively inhibited by a specific pore-targeting anti-ANO1 antibody and T16A$_{inh}$-A01. $I_{Cl.Ca}$ was recorded in mVMs respectively isolated from sham (A,a and B,a) and myocardial ischemic groups before (A,b and B,b) or after application of specific pore-targeting anti-ANO1 antibody and 30 μmol/L T16A$_{inh}$-A01 (A,c and B,c). (A,d and B,d) Summarized densities of $I_{Cl.Ca}$ were plotted as a function of membrane potentials under given conditions; $I_{Cl.Ca}$ was significantly up-regulated by myocardial ischemia and was dramatically inhibited by either specific pore-targeting anti-ANO1 antibody (n = 5) or T16A$_{inh}$-A01 (n = 5).

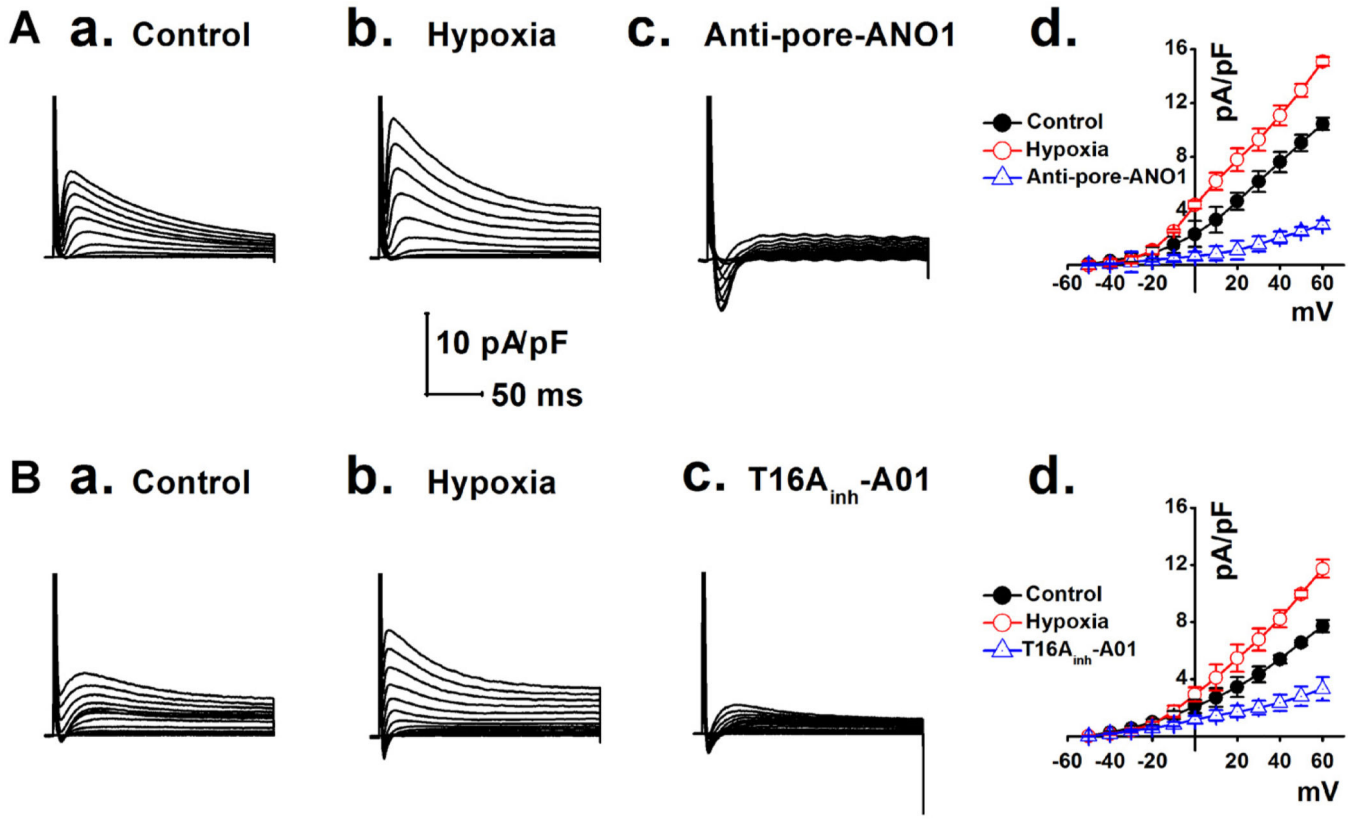

Fig. 6.

Representative $I_{Cl.Ca}$ was respectively recorded in the mVMs under the normoxic (A,a and B,a), hypoxic (A,b and B,b) conditions and in the presence of inhibitors (A,c and B,c). (A,d and B,d) Summarized densities of $I_{Cl.Ca}$ were plotted against membrane potentials; $I_{Cl.Ca}$ was significantly up-regulated by hypoxia and was dramatically inhibited by a specific pore-targeting anti-ANO1 antibody (n = 6) and T16A$_{inh}$-A01 (n = 5).

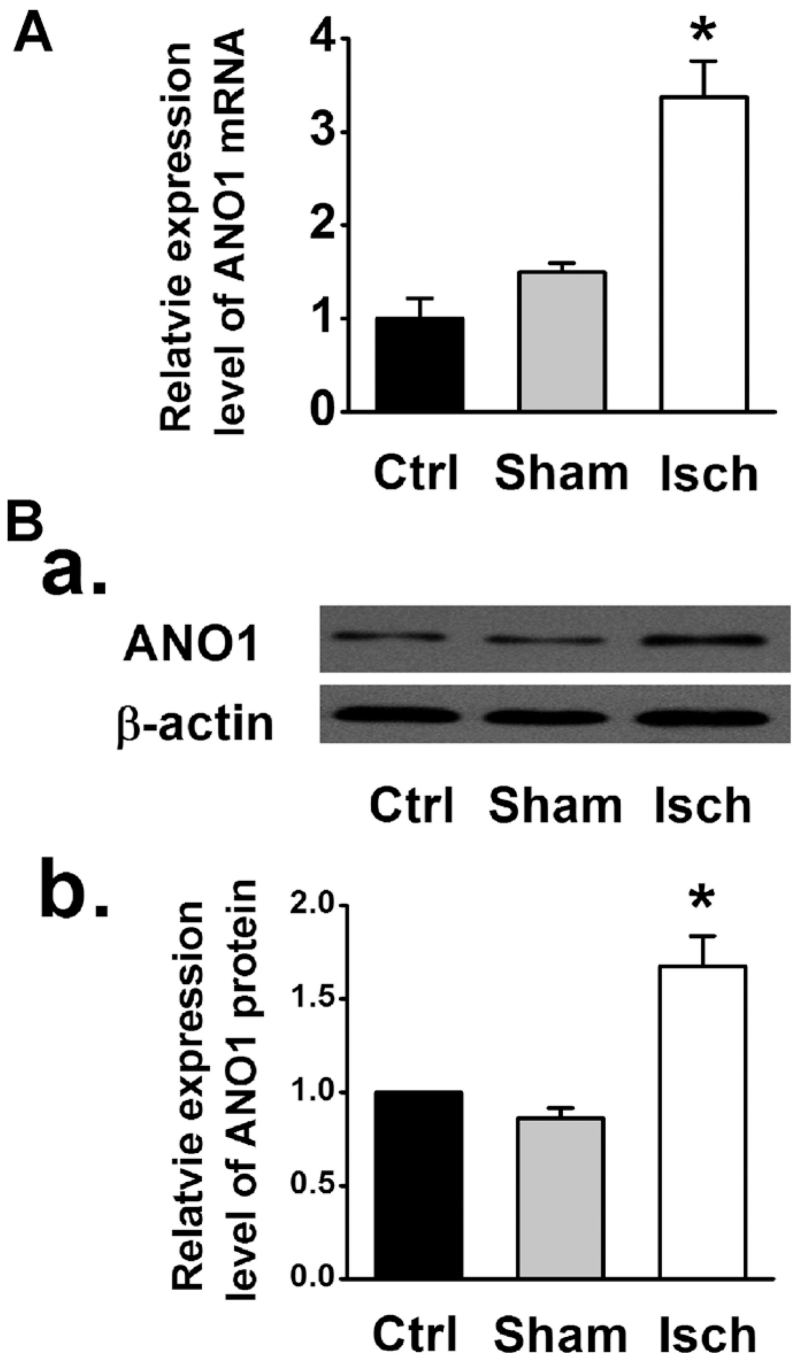

Fig. 7.

(A) Relative mRNA abundance of ANO1 examined by qRT-PCR in LV tissues from control (Ctrl), sham and myocardial ischemia (Isch) groups (n = 3). (B) Representative western blot (B,a) and averaged ANO1 protein densities in the isolated mVMs from control, sham, and myocardial ischemia group (B,b) (n = 5). * Indicates $P < 0.05$ *vs.* control or sham.

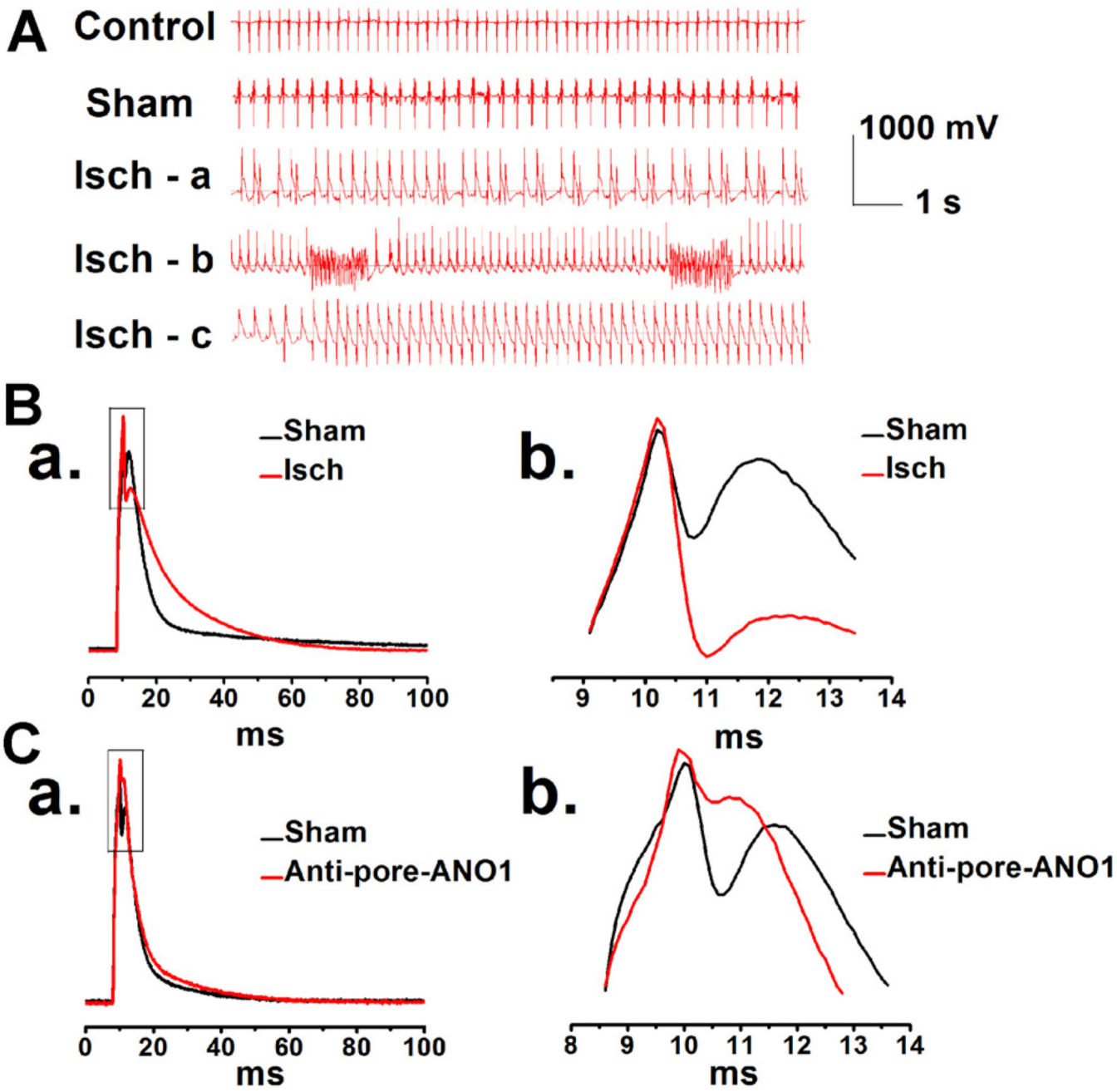

Fig. 8.

A. Representative ECG recordings in mice during surgeries. Isch-a: an example of ischemia with ventricular premature beats (VE); Isch-b: an example of ischemia with ventricular fibrillation (VF); Isch-c: an example of ischemia with ventricular tachycardia (VT). B. Representative APs were recorded in the mVMs isolated from sham (the black line) and myocardial ischemia (the red line) groups, respectively (B,a). Amplified portion of AP (square boxes in B,a) is shown in panel B,b. C. Representative APs were recorded in the same ventricular myocytes isolated from control mice, before (the black line) or after

application of specific pore-targeting anti-ANO1 antibody (the red line) (C,a). C,b. The enlarged portion indicated by square boxes in C,a.

TABLE 1

Oligonucleotide primers for qRT-PCR in this study

Primer	Gene Accession No.	Oligonucleotide Sequences (5'-3')	Amplicon Size
ANO1	NM_178642	AGGACCTGGGCTACCTGCCG (sense) CACATGCCAGGGCGCATGGA (antisense)	416 bp
ANO2	NM_153589	ATGCACTTTCACGACAACCA (sense) AAGTCCTTCTCCAGCTCCAG (antisense)	263 bp
GAPDH	NM_008084	CTGGAGAAACCTGCCAAGTA (sense) CTGTTGCTGTAGCCGTATTC (antisense)	224 bp

GAPDH, glyceraldehyde-3-phosphate dehydrogenase. All the primers correspond to *mus musculus*.

TABLE 2

Effects of ischemia and a specific pore-targeting anti-ANO1 antibody on APD in single mVMs

	APD_{20} (ms)		APD_{90} (ms)	
Frequency (Hz)	Sham (n = 8)	Ischemia (n = 8)	Sham (n = 8)	Ischemia (n = 8)
5	13.9 ± 0.2	10.9 ± 0.2*	31.4 ± 3.1	51.3 ± 5.9*
	APD_{20} (ms)		APD_{90} (ms)	
Frequency (Hz)	Control (*n* = 6)	ANO1 antibody (*n* = 6)	Control (*n* = 6)	ANO1 antibody (*n* = 6)
5	13.1 ± 0.3	15.3 ± 0.3€	33.2 ± 2.1	34.2 ± 1.8

APD_{20} and APD_{90} represent action potential duration to 20% and 90% of repolarization.

*$P < 0.01$ vs. Sham;

€$P < 0.01$ vs. Control.

TABLE 3

Effects of ischemia and a specific pore-targeting anti- ANO1 antibody on early phase of APD in single mVMs

	τ (ms)		τ (ms)	
Frequency (Hz)	**Sham (n = 8)**	**Ischemia (*n* = 8)**	**Control (*n* = 6)**	**ANO1 antibody (*n* = 6)**
5	1.9 ± 0.1	0.7 ± 0.1*	1.8 ± 0.1	2.9 ± 0.2€

τ represents the time constant of repolarization of APs from the peak of "spike" to the beginning of "dome".

*$P < 0.01$ vs. Sham;

€$P < 0.01$ vs. Control.